# Performance Enhancement of Permanent Magnet DC Motor with SEPIC Converter through Higher-order Sliding Surface

R. Dhanasekar, *Member, IEEE*, S. Ganesh Kumar, *Member, IEEE,* and Marco Rivera, *Member, IEEE*

***Abstract*— The primary concern of this article is to stabilize the rotating speed of a permanent magnet DC (PMDC) motor driven by a DC-DC SEPIC converter under mismatched disturbances via a higher order PID sliding surface (PIDSS) controller. This controller offers numerous benefits, including robustness, enhanced control performance, flexibility, simple implementation, and low cost. An algorithm for the above-mentioned control is developed to handle various load torques, including no-load, constant, frictional, and propeller types. Furthermore, the features of PIDSS are compared with classical sliding surface, sliding mode control (SMC) and proportional integral controller (PIC) by taking into consideration peak overshoot, steady-state error and settling time. Both simulation and experimental results are obtained satisfactorily.**

**Link to graphical and video abstracts, and to code: https://latamt.ieeer9.org/index.php/transactions/article/view/8811**

***Index Terms*—Higher order sliding mode control, PMDC motor, SEPIC converter, Sliding surface, Speed control**

## I. INTRODUCTION

DC-DC converters are commonly employed in communication devices, battery adapters, DC drives, distributed power supply systems, wireless power transmission, and electric vehicles [1-3]. Among the various DC-DC converters such as: buck/boost, Cuk and SEPIC converters have features in terms of efficiency, cost, and controller design complexity [4]. Among these converters, Cuk [5] and SEPIC converters [6] are employed in low ripple current applications. The demerit of the Cuk converter is its inverse polarity in the output voltage. SEPIC converter produces a similar output voltage to Cuk converter without reversing the output voltage [7]. SEPIC converter is employed in renewable applications [8-11], DC microgrid [12], voltage-doubler rectifier [13-14], switched reluctance motor [15-17], induction motor [18] and BLDC motor drive [19]. Nevertheless, the fourth order of SEPIC converter and its nonlinear structure leads to complexity in designing the controller to fulfil the robustness, fast response under transient conditions and stability.

Despite the fact that the SEPIC converter is involved with a wide variety of nonlinear controllers [20-22], among the above different controllers, the merits of sliding mode control (SMC) attract researchers in the field of controlling the converters, in applications such as aerospace, electric drives, electromechanical systems, robotics and electric vehicles. SMC has considerable merits such as: robustness, easy implementation and good response [23-24]. This approach employs a discontinuous control law to place and maintain the system motion on the designated sliding surface [25]. Despite its simplicity, first-order SMC generates high-frequency oscillations that degrade its effectiveness of the entire system. To eliminate such oscillations, higher-order sliding mode control (HOSMC) is employed. For better response and robustness of the control system, higher-order derivatives of the system's state elements are added to the sliding surface equation. HOSMC approach eliminates the chattering effect with the knowledge of variable's temporal derivatives [26-27]. In [28], higher order sliding mode control with various sliding surfaces is implemented for the buck converter with PMDC motor. The integral sliding approach has been confirmed to perform well in various applications including [29-31] (Fig.1).

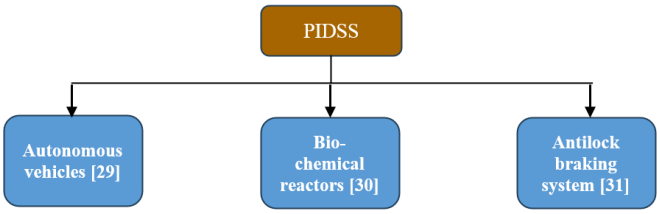


Fig.1. Applications of PIDSS.

Motivated by the above literature survey, this paper proposes the proportional derivative integral sliding surface (PIDSS) for a PMDC motor.

### *A. Contributions*

The following are the major contributions of this work:

- A PI derivative sliding surface (PIDSS) with second-order time derivative and second-order classical-sliding surface (CSS) are developed and put into effect of speed control for the PMDC motor via a fourth-order SEPIC converter.
- Restriction of the order of the sliding surface for implementation is realized by investigating via relative degree and order of the system.
- The behavior of the PIDSS controller is analyzed under varying the reference signal and load torque conditions.
- The proposed higher-order PIDSS controller improves the system's performance by reducing steady-state

R. Dhanasekar is with Sri Sairam Institute of Technology, Chennai, Tamilnadu, 600044, India (e-mail: rvdhanasekar@gmail.com).

S. Ganesh Kumar is with College of Engineering Gunidy, Anna University, Chennai, Tamilnadu, 600025, India (e-mail: ganeshkumar@annauniv.edu).

M. Rivera is with Universidad de Talca, Curicó, 3341717, Chile (e-mail: marcoriv@utalca.cl).

errors, peak overshoot and settling time, even under various load torque conditions.

### B. Paper Formation

The sequence of the chapters is as described below,

Section II explains the general design procedure for HOSMC, Section III explains the modelling and control of a SEPIC converter-fed PMDC motor, and Sections IV and V address the design of second-order CSS and PIDSS algorithms, respectively. The simulation and hardware outcomes are discussed in Sections VI and VII. This paper finishes with conclusions and generalized recommendations.

## II. Generalized Procedure for Designing HOSMC

This section describes the general method to derive the control input of HOSMC for a SEPIC converter-fed PMDC motor, ensuring that the state trajectories reach and reside on either CSS or PIDSS.

*Step 1: Description of the Non-linear System*

Consider a '$n^{th}$' order system with '$x_n$' as output variable and it is represented by a set of expressions as shown in (1).

$$\dot{x}_1(t) = G_{11}x_1(t) + G_{12}x_2(t) + \ldots\ldots + G_{1n}x_n(t) + B_{1n}u(t)$$
$$\dot{x}_2(t) = G_{21}x_1(t) + G_{22}x_2(t) + \ldots\ldots\ldots\ldots + G_{2n}x_n(t)$$
$$\ldots\ldots\ldots\ldots\ldots\ldots\ldots\ldots$$
$$\dot{x}_n(t) = G_{n1}x_1(t) + G_{n2}x_2(t) + \ldots\ldots\ldots + G_{nn}x_n(t) \quad (1)$$

Where $x_1(t), x_2(t) \ldots\ldots\ldots\ldots x_n(t)$ are the state parameters, u(t) is the control parameter and $G_{ij}$ are constant parameters, with i= 1 to n and j=1 to n. To design a HOSMC for the output variable '$x_n$', it is essential to fix the order of the sliding surface which is restricted by relative degree (D), as detailed below.

*Step 2: Identification of Relative Degree*

The relative degree (D) of '$n^{th}$' order system is calculated by differentiating the output term $'x_n(t)'$ continuously until control input 'u' reaches. The earliest derivative of the output term $'x_n(t)'$ is represented as follows:

$$\frac{dx_n}{dt} = f(x_n) + \text{constant term} \quad (2)$$

The second and subsequent derivatives of the output term $'x_n(t)'$ is given as,

$$\frac{d^{D-(n-2)}x_n}{dt^{D-(n-2)}} = f^{i=1}(x_n) + f(x_n) + \text{constant term}$$
$$= f^{I}(x_n) + f(x_n) + \text{constant term} \quad (3)$$
$$\frac{d^{D-(n-3)}x_n}{dt^{D-(n-3)}} = f^{i=D-(n-2)}(x_n) + f^{i=1}(x_n) + \text{constant term}$$
$$= f^{II}(x_n) + f^{I}(x_n) + \text{constant term} \quad (4)$$

$$\frac{d^{D}x_n}{dt^{D}} = f^{i=D}(x_n) + b_{1n}u + \text{constant term} \quad (5)$$

At $D^{th}$ time derivative ($D \leq n$), the control input 'u' appears which confirms the system's relative degree as 'D'. From this, the order of sliding surface can be computed by using the formula (D-1).

*Step 3: Sliding Surface Identification and Computation of its Derivatives*

HOSMC is designed to reach the desired condition $'x_d'$, for the output variable $'x_n'$, by reducing the error $'e_r'$ between them. The sliding surface is designed with required control input, so that the $r^{th}$ order sliding mode is enforced on the sliding surface in such a way that,

$$\text{i.e. } S(e_r, \dot{e_r}) = \dot{S}(e_r, \dot{e_r}) = \ldots\ldots\ldots\ldots\ldots S^{r-1}(e_r, \dot{e_r}) = 0$$

Derivatives are computed and represented in the equations from (6) to (8).

$$\dot{S}(e_r, \dot{e_r}) = \frac{\partial S(e_r, \dot{e_r})}{\partial x_n} = f^{I}(e_r, \dot{e_r}) + \text{constant term} \quad (6)$$

$$\ddot{S}(e_r, \dot{e_r}) = \frac{\partial^2 S(e_r, \dot{e_r})}{\partial {x_n}^2} = f^{II}(e_r, \dot{e_r}) + f^{I}(e_r, \dot{e_r}) + \text{constant term} \quad (7)$$

$$\ldots\ldots\ldots\ldots\ldots\ldots\ldots\ldots\ldots\ldots\ldots\ldots\ldots\ldots$$
$$\overset{D-1}{S(e_r, \dot{e_r})} = \frac{\partial^{D-1} S(e_r, \dot{e_r})}{\partial {x_n}^{D-1}} = f^{D-1}(e_r, \dot{e_r}) +$$
$$f^{D-2}(e_r, \dot{e_r}) + \ldots\ldots f^{I}(e_r, \dot{e_r}) + b_{1n}u + \text{constant term} \quad (8)$$

The control input 'u' appears at the sliding order (D-1).

*Step 4: Generation of Equivalent (continuous) Signal '$u_{eq}$'*

In order to compute the continuous signal $'u_{eq}'$, equation (8) is equated to zero which is shown in equation (9).

$$\overset{D-1}{S(e_r, \dot{e_r})} = f^{D-1}(e_r, \dot{e_r}) + f^{D-2}(e_r, \dot{e_r}) + \cdots\ldots\ldots f^{I}(e_r, \dot{e_r}) +$$
$$b_{1n}u + \text{constant term} = 0 \quad (9)$$

Making $\overset{D-1}{S(e_r, \dot{e_r})} = 0$ and replacing 'u' as '$u_{eq}$', then the sliding surface equation will become,

$$u_{eq} = [f^{D-1}(e_r, \dot{e_r}) + f^{D-2}(e_r, \dot{e_r}) + \ldots\ldots\ldots\ldots f^{I}(e_r, \dot{e_r}) +$$
$$\text{constant term}]\,[b_{1n}]^{-1} \quad (10)$$

*Step 5: Selection of Switching Signal $'u_{sw}'$*

The switching signal $'u_{sw}'$ is obtained by the following general equation [33],

$$N_{ir} = \{|S|^{q/r} + \left|\frac{ds}{dt}\right|^{q/r-1} + \ldots. + \left|(S^{i-r})\right|^{q/r-i+1}\}^{(r-i/q)} \quad (11)$$

where,

q is the least common multiple of '1' to 'r', where 'r' is the sliding order and i= 1……(r-1).

$$\varphi_{0r} = \text{sign}(S) \quad (12)$$
$$\varphi_{ir} = \text{sign}(S^{(i)} + \beta_i N_{ir}\varphi_{i-1,r}) \quad (13)$$

The switching signal for the $r^{th}$ order sliding controller is given as,

$$u_{sw} = -\alpha\, \varphi_{r-1,r}\,(S, \dot{S} \ldots\ldots\ldots\ldots\ldots\ldots S^{r-1}) \quad (14)$$

Select the control parameters $\alpha > 0$ *and* $\beta_i > 0$, such that the control scheme is made to sustain in finite time.

*Step 6: Final Control Law*

Make the resultant control law as; $u = u_{eq} + u_{sw}$ which comprises two signals added together; the continuous parameter $'u_{eq}'$ and the discontinuous parameter $'u_{sw}'$. Finally, the control expressions for 'u' in the CSS and PIDSS are as follows:

$$u = -[f^{D-1}(e_r, \dot{e_r}) + f^{D-2}(e_r, \dot{e_r}) + \ldots\ldots\ldots\ldots f^{I}(e_r, \dot{e_r}) + \text{constant term}]\,[b_{1n}]^{-1}] + u_{sw} \quad (15)$$

Finally, the control parameter 'u' for PIDSS is expressed as,

$$u = [-[D_1(\dot{e_r}) + D_2(e_r) + D_3(\ddot{e}_r)\ \text{constant term}] + [b_{1n}]^{-1}] + u_{sw} \quad (16)$$

## III. Modeling of PMDC Motor Powered By SEPIC Converter

Fig. 2 displays the setup of HOSMC implementation for the SEPIC converter and PMDC motor combination. The circuit includes the input supply as '$V_{in}$ = 6 V', control switch '$S_W$' as MOSFET, inductors '$L_1$= 0.1333 mH', '$L_2$ = 0.1333 mH', capacitors '$C_1$ = 10 µF', '$C_2$ = 700 µF' and diode '$D_D$'. The proposed system's state parameters are the currents flowing through the two inductors ($i_{L1}$ & $i_{L2}$), voltages across the two capacitors ($v_{c1}$ & $v_a$), armature current ($i_a$) and motor speed ($\omega$). The control input signal is derived using HOSMC technique based on the feedback from speed, armature voltage, armature current and inductor currents. The state space equations for the SEPIC converter with PMDC motor are given as,

$$\frac{di_{L1}}{dt} = \frac{V_{in}}{L_1} - (1-u)\frac{(v_{c1}+v_a)}{L_1} \quad (17)$$

$$\frac{di_{L2}}{dt} = \frac{v_{c1}}{L_2}u - (1-u)\frac{v_a}{L_2} \quad (18)$$

$$\frac{dv_{c1}}{dt} = \frac{(1-u)i_{L1}}{C_1} - \frac{i_{L2}}{C_1}u \quad (19)$$

$$\frac{dv_a}{dt} = \frac{(i_{L1}+i_{L2})}{C_2}(1-u) - \frac{i_a}{C_2} \quad (20)$$

$$\frac{d\omega}{dt} = -\frac{B}{J}\omega + \frac{K_t}{J}i_a - \frac{T_L}{J} \quad (21)$$

$$\frac{di_a}{dt} = -\frac{K_e}{L_a}\omega - \frac{R_a}{L_a}i_a + \frac{v_a}{L_a} \quad (22)$$

where,

| | |
|---|---|
| $\omega$ | Speed of the motor - rad/sec |
| $i_a$ | Armature current - Amperes |
| $T_L$ | Load torque – (N·m) |
| J | Moment of Inertia - kgm$^2$ |
| $v_a$ | Armature voltage - V |
| $v_{c1}$ | Capacitor voltage - V |
| $V_{in}$ | Voltage input to the SEPIC converter - V |
| $i_{L1}$,$i_{L2}$ | Inductor current - Amperes |
| $K_t$ | Constant of motor torque (N·m/Ampere) |
| $K_e$ | Constant of back emf of the motor (V /rpm) |
| $R_a$ | Armature resistance - Ohms |
| $L_a$ | Armature inductance - Henry |

The switch '$S_W$' is controlled by the control input 'u'. The steady state values for $i_a$,$v_a$and u for the reference speed are given by (23) to (25),

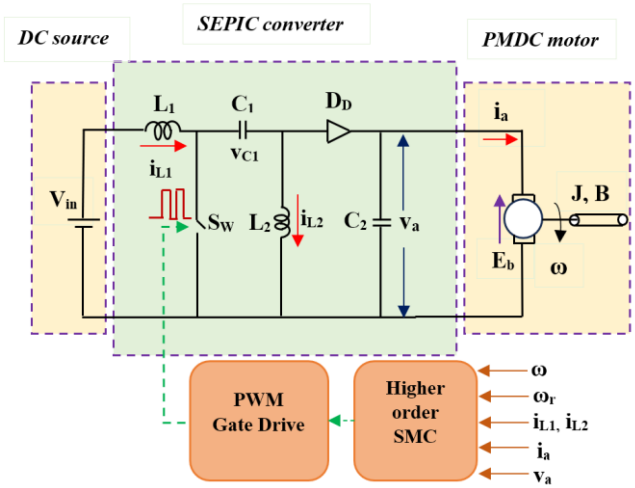


Fig.2. Circuit diagram of SEPIC converter.

$$i_{a_{ss}} = \frac{B\omega_r}{K_t} + \frac{T_L}{K_t} \quad (23)$$

$$v_{a_{ss}} = K_e\omega_r + R_a i_{a_{ss}} \quad (24)$$

$$u_{ss} = \frac{v_{a_{ss}}}{v_{a_{ss}}+V_{in}} \quad (25)$$

## IV. Design of Second-Order SMC with CSS

The classical sliding surface (CSS) is denoted as "δ " and is defined by equation (26). It drives the system states to converge towards their intended values.

$$\delta = Ce_r + \frac{de_r}{dt} \quad (26)$$

Here the speed error '$e_r$' is the deviation between the speed reference '$\omega_{ref}$' and the actual speed '$\omega$'. 'C' is the positive real number.

The derivative of equation (26) can be written as follows,

$$\frac{d\delta}{dt} = \omega(\lambda_1) + i_a(\lambda_2) - \frac{K_t}{JL_a}v_a + T_L\left(\frac{C}{J} - \frac{B}{J^2}\right) \quad (27)$$

where,

$$\lambda_1 = \left(C\frac{B}{J} + \frac{K_t}{J}\frac{K_e}{L_a} + \frac{B^2}{J^2}\right);\ \ \lambda_2 = \left(\frac{K_t}{J}\frac{R_a}{L_a} - C\frac{K_t}{J} + \frac{BK_t}{J^2}\right)$$

$$\frac{d}{dt}\left(\frac{d\delta}{dt}\right) = \omega\left(-\frac{B}{J}\lambda_1 - \lambda_2\frac{K_e}{L_a}\right) + i_a\left(\frac{K_t}{J}\lambda_1 - \frac{R_a}{L_a}\lambda_2 + \frac{K_t}{JC_2L_a}\right) - \frac{\lambda_2}{L_a}v_a - (i_{L1}+i_{L2})\frac{K_t}{JC_2L_a} + u(i_{L1}+i_{L2})\frac{K_t}{JC_2L_a} - T_L\frac{\lambda_1}{J} \quad (28)$$

The system steps in to the sliding condition when $\frac{d}{dt}\left(\frac{d\delta}{dt}\right) = 0$. The equivalent control signal can be acquired by making

$\frac{d}{dt}\left(\frac{d\delta}{dt}\right) = 0$ and 'u' as '$u_{eq}'$ in equation (28) and the following term arises as,

$$u_{eq} = \left[\omega\left(-\frac{B}{J}\lambda_1 - \lambda_2\frac{K_e}{L_a}\right) + i_a\left(\frac{K_t}{J}\lambda_1 - \frac{R_a}{L_a}\lambda_2 + \frac{K_t}{JC_2L_a}\right) - \frac{\lambda_2}{L_a}v_a - (i_{L1}+i_{L2})\frac{K_t}{JC_2L_a} - T_L\frac{\lambda_1}{J}\right]/(i_{L1}+i_{L2})\frac{K_t}{JC_2L_a} \quad (29)$$

Using an approach based on homogeneity, finite-time convergence is attained [32]. The generation of switching signal is attained by considering r=2, i=1 and q= 2.

Substitute the values of 'r', 'q' and 'i' in (11), (12), (13) and (14), the expressions become,

$$N_{12} = (|\delta|)^{(1/2)} \quad (30)$$

$$\varphi_{02} = \text{sign}\,(\delta) \quad (31)$$

$$\varphi_{12} = \text{sign}\,(\dot{\delta} + \beta_1 N_{12}\varphi_{02}) \quad (32)$$

The switching signal for the higher (second) order sliding controller is given as,

$$u_{sw} = -\alpha(\text{sign}\,(\dot{\delta} + \beta_1((|\delta|)^{(1/2)})(\text{sign}\,(\delta)\,))) \quad (33)$$

$$u_{sw} = -\alpha\text{sign}(\dot{\delta} + \beta_1 N_{12}\varphi_{02}) \quad (34)$$

The control law for the SEPIC converter fed PMDC motor is finalized as,

$$u = u_{eq} + u_{sw} \quad (35)$$

$$u = \{\left[\omega\left(-\frac{B}{J}\lambda_1 - \lambda_2\frac{K_e}{L_a}\right) + i_a\left(\frac{K_t}{J}\lambda_1 - \frac{R_a}{L_a}\lambda_2 + \frac{K_t}{JC_2L_a}\right) - \frac{\lambda_2}{L_a}v_a - (i_{L1}+i_{L2})\frac{K_t}{JC_2L_a} - T_L\frac{\lambda_1}{J}\right]/(i_{L1}+i_{L2})\frac{K_t}{JC_2L_a}\} + \{-\alpha\text{sign}(\dot{\delta} + \beta_1 N_{12}\varphi_{02})\} \quad (36)$$

Using the trial-and-error method [33], the sliding parameter 'C' is set to 5.2 in the second-order CSS so that the speed characteristic is adequate and unaltered. The control values 'α' and '$\beta_1$' are selected as $50*10^4$ and 1850.

## V. Design of Second Order SMC with PIDSS

For regulating the PMDC motor's speed under varying load torque circumstances, proportional, integral, and derivative parameters are incorporated into the PIDSS of the speed error ($e_r$).

$$e_r = \omega_{ref} - \omega \quad (37)$$

Where '$\omega_{ref}$' is the speed reference and '$\omega$' is the actual speed. PIDSS is written as,

$$\varphi = D_1(e_r) + D_2\int e_r\,dt + D_3\frac{d(e_r)}{dt} \quad (38)$$

Where $D_1$, $D_2$ ,$D_3$ are proportional-integral-derivative gains

The first derivative of '$\varphi$' is given as in (39).

$$\frac{d\varphi}{dt} = \omega\alpha_1 + i_a\alpha_2 + \alpha_3 v_a + T_L\left(D_1\frac{1}{J} - D_3\frac{B}{J^2}\right) + D_2(e) \quad (39)$$

where,

$$\alpha_1 = \left(D_1\frac{B}{J} + D_3\frac{K_t}{J}\frac{K_e}{L_a} - D_3\frac{B^2}{J^2}\right);\ \alpha_2 = \left(D_3\frac{K_t}{J}\frac{R_a}{L_a} - D_1\frac{K_t}{J} + D_3\frac{BK_t}{J^2}\right)$$

$$\alpha_3 = -D_3\frac{K_t}{JL_a}$$

The second derivative of (39) is represented in (40).

$$\frac{d}{dt}\left(\frac{d\varphi}{dt}\right) = \omega\left(-\frac{B}{J}\alpha_1 - \frac{K_e}{L_a}\alpha_2 + \frac{B}{J}\alpha_3\right) + i_a\left(\frac{K_t}{J}\alpha_1 - \frac{R_a}{L_a}\alpha_2 - \frac{K_t}{J}D_2 - \frac{1}{C_2}\alpha_3\right) + \frac{\alpha_2}{L_a}v_a - (i_{L1}+i_{L2})\frac{\alpha_3}{C_2}u + (i_{L1}+i_{L2})\frac{\alpha_3}{C_2} + T_L\left(\frac{D_2}{J} - \frac{\alpha_1}{J}\right) \quad (40)$$

The equivalent control input is fixed by making $\frac{d}{dt}\left(\frac{d\varphi}{dt}\right) = 0$ and 'u' as '$u_{eq}$' in (40), then (41) arises.

$$u_{eq} = \left[\omega\left(-\frac{B}{J}\alpha_1 - \frac{K_e}{L_a}\alpha_2 + \frac{B}{J}\alpha_3\right) + i_a\left(\frac{K_t}{J}\alpha_1 - \frac{R_a}{L_a}\alpha_2 - \frac{K_t}{J}D_2 - \frac{1}{C_2}\alpha_3\right) + \frac{\alpha_2}{L_a}v_a + (i_{L1}+i_{L2})\frac{\alpha_3}{C_2} + T_L\left(\frac{D_2}{J} - \frac{\alpha_1}{J}\right)\right]/(i_{L1}+i_{L2})\frac{\alpha_3}{C_2} \quad (41)$$

Using the homogeneity method, finite-time convergence is attained [32]. The switching signal '$u_{sw}$' is represented as,

$$u_{sw} = -\alpha\text{sign}(\dot{\varphi} + \beta_1((|\varphi|)^{(1/2)})(\text{sign}\,(\varphi))) \quad (42)$$

The control law for the SEPIC converter fed PMDC motor is finalized as,

$$u = u_{eq} + u_{sw} \quad (43)$$

$$u = \left[\omega\left(-\frac{B}{J}\alpha_1 - \frac{K_e}{L_a}\alpha_2 + \frac{B}{J}\alpha_3\right) + i_a\left(\frac{K_t}{J}\alpha_1 - \frac{R_a}{L_a}\alpha_2 - \frac{K_t}{J}D_2 - \frac{1}{C_2}\alpha_3\right) + \frac{\alpha_2}{L_a}v_a + (i_{L1}+i_{L2})\frac{\alpha_3}{C_2} + T_L\left(\frac{D_2}{J} - \frac{\alpha_1}{J}\right)\right]/(i_{L1}+i_{L2})\frac{\alpha_3}{C_2} + (-\alpha\text{sign}(\dot{\varphi} + \beta_1((|\varphi|)^{(1/2)})(\text{sign}\,(\varphi)))) \quad (44)$$

The values of $D_1$, $D_2$ and $D_3$ are selected as 13, 0.3 and 0.15 respectively. The value of control parameters α and $\beta_1$ are $25*10^{100}$ and 18000.

## VI. Simulation Analysis

TABLE I
PMDC Motor Parameters

| PMDC motor parameter | Value |
|---|---|
| $P_o$: Power | 18 W |
| $V_a$: Voltage | 12 V |
| $I_a$: Current | 1.5 A |
| T: Torque | 1 kg cm |
| $R_a$: Armature resistance | 2.6 Ω |
| $L_a$: Armature inductance | 712.85 mH |
| $K_e$: Backemf constant | 0.05022 V s/rad |
| J: Moment of Inertia | 88.6138e-6 kgm$^2$ |
| B: coefficient of viscous friction | 96.894e-6 N·m/rad |
| $K_e$: Constant value of Torque | 0.05022 N·m/A |
| ω: Speed | 157 rad/sec |

Through MATLAB simulation, the effective operation of the PI controller (PIC), SMC, second order SMC with CSS and PIDSS under second-order are demonstrated for various load torque constraints as listed in Table I. The feedback inputs used for HOSMC include the motor's actual speed, current through armature, armature voltage and the inductor currents of the converter.

Table II outlines the machine's functioning parameters for the specified speed pattern and load torque pattern. For the chosen speed (Fig. 3) and torque pattern (Fig. 4), the converter operates under buck/boost mode.

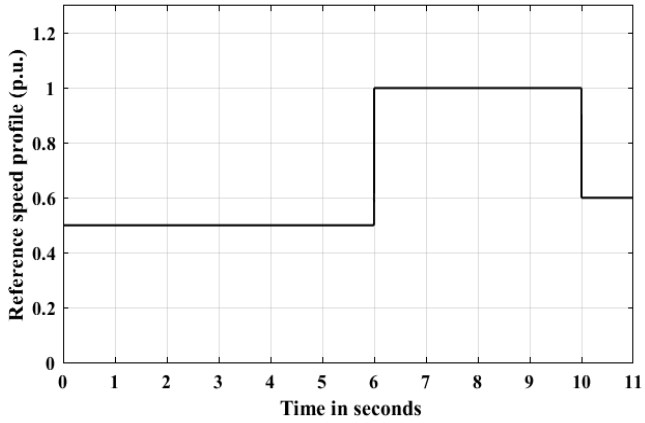


Fig.3. Selected speed profile in per unit.

TABLE II
SPECIFICATIONS OF MACHINE BEHAVIOR

| Time (secs) | Speed reference Pattern (p.u.) | Load torque Pattern (p.u.) |
|---|---|---|
| 0 to 4 | 0.5 | - |
| 4 to 6 | 0.5 | 0.5 |
| 6 to 8 | 1 | 0.5 |
| 8 to 10 | 1 | 1 |
| 10 to 11 | 0.6 | 1 |

The effect of PIC, SMC, and second order SMC with CSS and PIDSS is evaluated under the range of the torques including constant, frictional, fan and propeller type.

### *A. Performance Under Constant Load Torque Conditions*

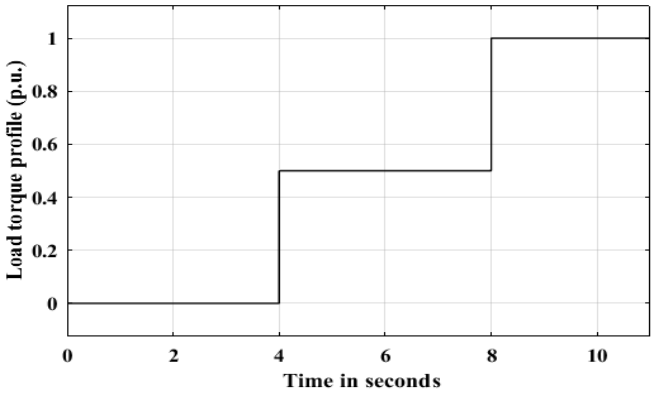


Fig.4. Selected load torque profile in per unit.

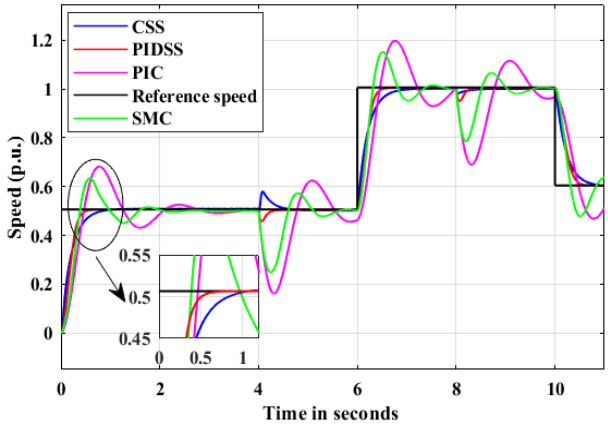


Fig.5. Speed responses for various reference speeds and load torques.

Fig. 5 depicts the speed behaviors of various higher-order sliding surfaces and other controllers as mentioned earlier. Between 0 and 6 seconds, the converter operates in buck mode, and between 6 and 12 seconds, it operates in boost mode.

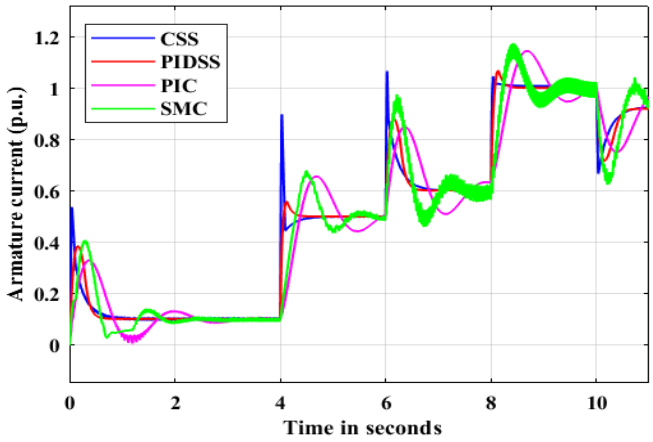


Fig.6.Comparison between PIC, SMC, second order SMC with CSS and PIDSS (Armature current changes for constant load torque).

Fig. 6 compares the armature current for PIC, SMC, second-order SMC with CSS, and PIDSS under the load torque with constant circumstance. The performance of second-order SMC with PIDSS is found to be superior to that of PIC, SMC and second order CSS.

### *B. Performance Under Frictional Torque Conditions*

Under frictional load torque, the relationship between torque and speed is given by $T_L = K\omega$, where K is $6.24e^{-3}$. The frictional load torque is sketched as follows: 0.5 p.u. between 0 and 6 seconds, 1 p.u. between 6 and 10 seconds, and 0.6 p.u. between 10 and 12 seconds. Fig. 7 demonstrates the duration required for the PMDC motor speed to stabilize is lower for second-order SMC with PIDSS when compared to PIC, SMC, and CSS with second-order.

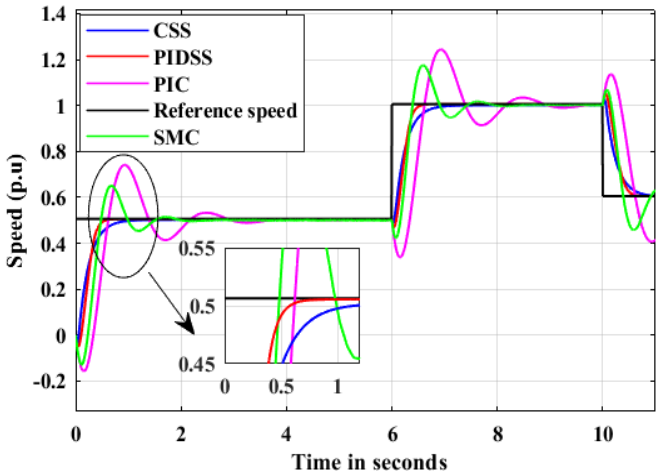


Fig.7. Speed response comparative study between PIC, SMC, second order SMC using CSS and PIDSS for the torque at frictional load.

### *C. Performance Under Fan Torque Conditions*

For the load torque due to fan load (Fig. 8), $T_L = K_2\omega^2$. The proportional representation constant $K_2$ is chosen as $2.44e^{-6}$. As depicted in Fig. 9, the PMDC motor's settling speed and speed tracking are superior for second-order SMC with PIDSS compared to second-order SMC with CSS, SMC, and PIC.

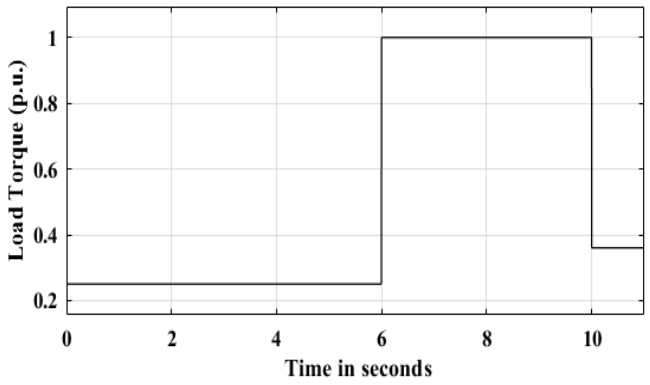


Fig.8. Fan type load torque profile.

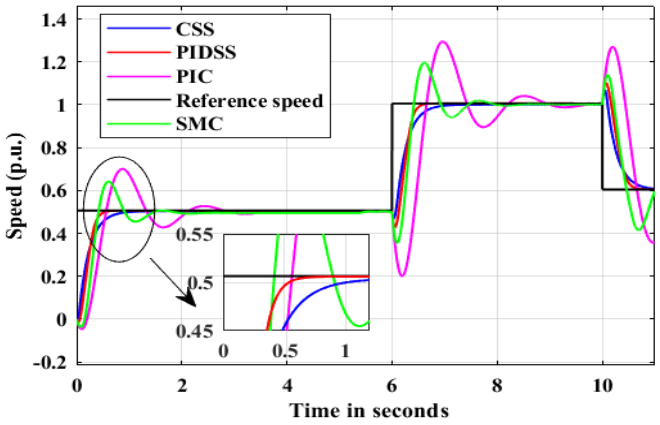


Fig.9. Speed responses for various reference speeds under fan load torque.

### *D. Performance Under Propeller Torque Conditions*

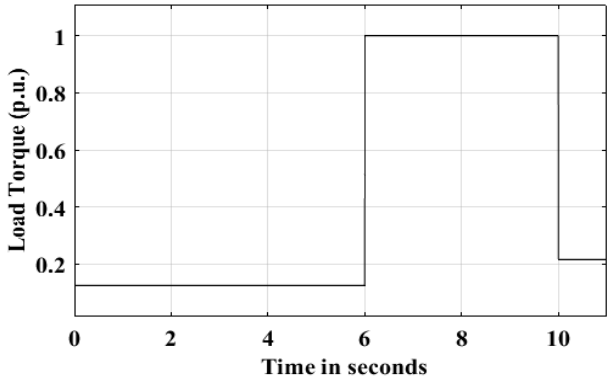


Fig.10. Propeller type load torque profile.

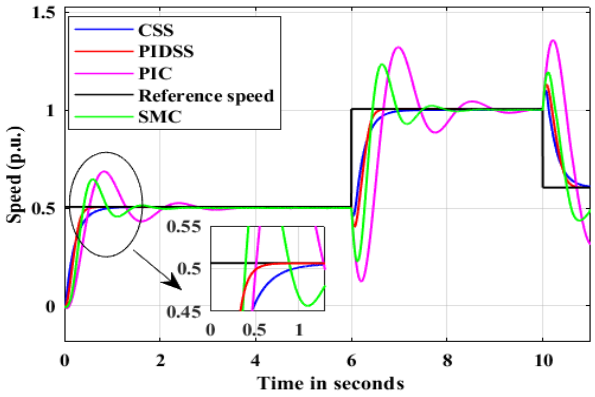


Fig.11. Speed responses for various reference speeds under propeller load torque.

Torque exhibits a direct relationship with speed for propeller loads i.e., ($T_L = K_3\omega^3$). $1.55e^{-8}$ is obtained as the value of the proportionality constant $K_3$. For the reference speed pattern as depicted in Fig. 3, the obtained load torque appears in Fig. 10. Fig. 11 illustrates the speed evolutions of the second-order SMC with PIDSS, CSS, SMC, and PIC. The comparison of speed settling durations is shown in Table III.

The aforementioned simulation study clearly shows that for servo tasks and regulatory activities of the PMDC motor, second-order SMC with PIDSS settles more quickly than second-order SMC using CSS, PIC, and SMC.

## VII. Experimental Setup and Discussions

Fig. 12 depicts the experimental framework for a PMDC motor integrated with SEPIC converter. The framework includes essential components such as: a 100 MHz digital storage oscilloscope, a 6V DC input source, a PMDC motor, a power converter circuit, and an FPGA (Field-Programmable Gate Array) controller. Measurements are taken using HEDS5645 sensor for motor speed, the 7840-voltage sensing IC for armature voltage, and the HEO55T01 for armature current. Spartan-6 XC6SCX9 is programmed and uploaded with control algorithms using Xilinx. A gate pulse activates the IGBT switch "S" (FGA25N120) in the SEPIC converter once uploading is complete and thus the speed of the motor is regulated.

An experimental configuration with a PMDC motor blending with a SEPIC converter is tested for constant load torque situations at an initial reference speed of 750 rpm., i.e., 50% of the rated speed, followed by take-offs to the rated rpm and descents to 900 rpm, i.e., 60% of the motor rated speed. Fig. 13 and Fig. 14. depicts the hardware outputs for CSS and PIDSS, respectively. Fig. 13 shows the consolidated results of reference speed, actual speed, current through the armature and armature voltage for the CSS under the conditions of constant load torque. At 750 rpm, the SEPIC converter operates in buck mode, whereas at 900 rpm and 1500 rpm, it operates in boost mode. Based on Fig. 13, the motor's settling time is becoming slow with steady-state error.

TABLE III
COMPARISON OF PIC, SMC, SECOND ORDER CSS AND SECOND ORDER PIDSS

| Time (seconds) | Reference speed (rad/sec) | Speed reference (p.u.) | Load torque $T_L$ (p.u.) | Speed - settling duration (secs) | | | | Steady-state error % | | | | Peak overshoot% | | | |
|---|---|---|---|---|---|---|---|---|---|---|---|---|---|---|---|
| | | | | 2nd order | | SMC | PIC | 2nd order | | SMC | PIC | 2nd order | | SMC | PIC |
| | | | | PIDSS | CSS | | | PIDSS | CSS | | | PIDSS | CSS | | |
| *a) load torque under constant circumstances* | | | | | | | | | | | | | | | |
| 0.0 – 4.0 | 78.5 | 0.5 | 0 | 0.571 | 0.972 | 2.458 | 3.569 | - | - | 0.15 | 0.2 | - | - | 13.5 | 18.6 |
| 4.0 – 6.0 | 78.5 | 0.5 | 0.5 | 0.35 | 0.65 | 1.641 | - | - | - | - | - | - | - | 7.7 | 12 |
| 6.0 -8.0 | 157 | 1 | 0.5 | 0.650 | 1.77 | 1.763 | - | - | - | - | - | - | - | 15 | 20 |
| 8.0 -10.0 | 157 | 1 | 1 | 0.382 | 0.555 | 1.574 | - | - | - | 0.8 | - | - | - | 6.6 | 11.7 |
| 10.0 -11.0 | 94.2 | 0.6 | 1 | 0.594 | 0.941 | - | - | - | - | - | - | - | - | - | - |
| *b) load torque under Frictional circumstances* | | | | | | | | | | | | | | | |
| 0.0 - 6.0 | 78.5 | 0.5 | 0.5 | 0.626 | 1.051 | 2.334 | 3.608 | - | - | 0.2 | - | - | - | 15.3 | 24.6 |
| 6.0- 10.0 | 157 | 1 | 1 | 0.571 | 1.043 | 1.986 | 3.614 | - | - | 0.2 | - | - | - | 17.8 | 25 |
| 10.0- 11.0 | 94.2 | 0.6 | 0.6 | 0.665 | 0.946 | - | - | - | - | - | - | - | - | - | - |
| *c) load torque under fan type circumstances* | | | | | | | | | | | | | | | |
| 0.0 - 6.0 | 78.5 | 0.5 | 0.25 | 0.587 | 0.988 | 2.196 | 3.615 | - | - | 0.5 | 0.3 | - | - | 14.7 | 20.7 |
| 6.0 - 10.0 | 157 | 1 | 1 | 0.673 | 1.028 | 1.942 | 3.687 | - | - | 0.2 | - | - | - | 19.6 | 29.5 |
| 10.0- 11.0 | 94.2 | 0.6 | 0.36 | 0.681 | 1.004 | - | - | - | - | - | - | - | - | - | - |
| *d) load torque under propeller type circumstances* | | | | | | | | | | | | | | | |
| 0.0 - 6.0 | 78.5 | 0.5 | 0.125 | 0.571 | 0.870 | 2.335 | 3.540 | - | - | 0.2 | 0.3 | - | - | 14.7 | 19.1 |
| 6.0 - 10.0 | 157 | 1 | 1 | 0.657 | 1.075 | 2.203 | 3.697 | - | - | 0.4 | 0.6 | - | - | 23.9 | 32.2 |
| 10.0- 11.0 | 94.2 | 0.6 | 0.216 | 0.673 | 1.043 | - | - | - | - | - | - | - | - | - | - |

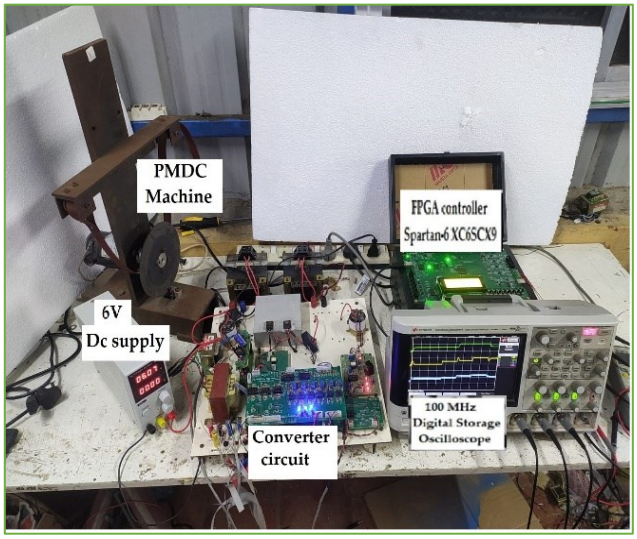


Fig.12. Prototype configuration for SEPIC converter fed PMDC motor.

The integrated results for voltage, current, and speed for the second-order SMC with PIDSS are illustrated in Fig. 14. PIDSS outperforms CSS regarding settling time and steady-state error. In both buck and boost modes, variations in speed, armature current, and armature voltage reveal the robustness of the higher-order PIDSS with reduced settling time and without steady state error. Regarding disturbance mitigation and performance recovery time, the PIDSS algorithm outperforms other approaches. Additionally, it can be seen that the suggested method does not exhibit any chattering. This implies that the suggested controller can regulate the speed regardless of the different loads applied. As shown in Table IV, the hardware implementation offers precise data on peak overshoot, steady-state error, and settling time. According to Table IV, PIDSS provides outstanding speed tracking performance under various load conditions both in buck and boost modes. In some systems, sliding surfaces with higher order proportional integral derivatives can provide sophisticated control features, but also have drawbacks such as; challenges in tuning the parameters, reduction in physical clarity and implementation complexity.

The proposed control strategy is suitable for renewable energy systems, medical devices, industrial automation, electric vehicles, and other applications where it requires improved system robustness and efficiency. PMDC motors' small size and accurate control via higher-order sliding surface methods make them ideal for effective and miniaturized electromechanical systems. To further enhance the potential of this integrated technology, future research will focus on investigating sophisticated control algorithms, fault-tolerant features, energy storage integration, and the coordination of numerous PMDC motors in multi-actuator systems.

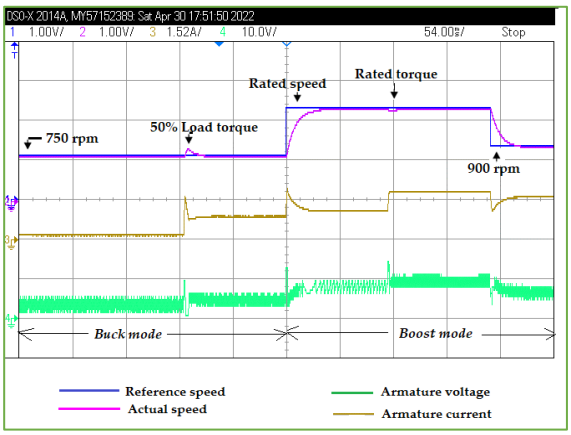


Fig.13. Responses of motor Speed, motor armature current and motor armature voltage changes for second-order SMC with CSS.

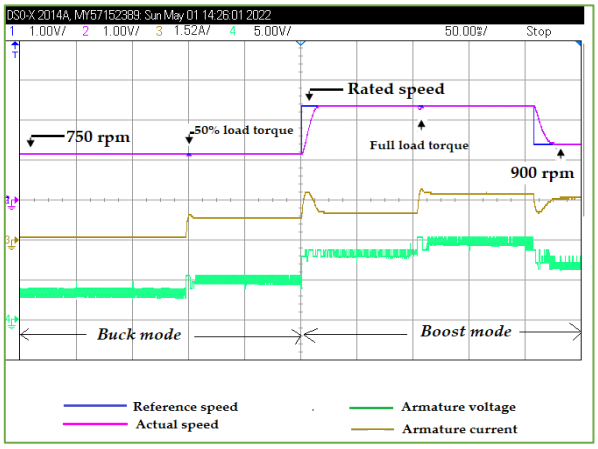


Fig.14. Responses of motor Speed, motor armature current and motor armature voltage changes for second-order SMC with PIDSS.

TABLE IV
COMPARISON OF SECOND-ORDER SMC AGAINST CSS AND PIDSS IN PRACTICAL CONFIGURATION FOR THE TORQUE AT CONSTANT LOAD SITUATION

| Variations in Speed reference (rad/sec) | Variations in Speed reference (p.u.) | Load Torque $T_L$ (p.u.) | Mode | Settling time of speed (seconds) | |
|---|---|---|---|---|---|
| | | | | PIDSS | CSS |
| 78.5 | 0.5 | 0.5 | Buck | 0.4 | 0.75 |
| 157 | 1 | 0.5 | Boost | 0.75 | 2.55 |
| 157 | 1 | 1 | Boost | 0.5 | 0.65 |
| 94.2 | 0.6 | 1 | Boost | 0.7 | 1.5 |

## VIII. CONCLUSION

In this paper, generalized procedures for the construction of control signal using higher order sliding mode control with Proportional Integral Derivative Sliding Surface (PIDSS) and Classical Sliding Surface (CSS) algorithms are developed. In continuation of that, above said algorithms are developed for SEPIC converter with PMDC motor load and MATLAB is used for the simulation of SEPIC converter with dynamic load for constant, frictional, fan type, and propeller load torques respectively. Simulation results indicate the exemplary performance of PIDSS in comparison with CSS, SMC and PIC. Further, an experimental setup is built for verifying the above under constant load torque conditions and the results are obtained satisfactorily. Hence, the proposed method has been shown to be effective in both the estimation and rejection of disturbances. The suggested controller demonstrates robustness by eliminating steady-state error, reducing peak overshoot, and minimizing settling time. Moreover, it operates without any visible chattering. As the results are promising, the proposed control can be extended in the future for various higher-order converters and loaded situations.

## ACKNOWLEDGMENTS

Authors thank DEEE, College of Engineering Guindy, Anna University, Tamilnadu, India for the financial support through the thematic area “Development of Energy Efficient Motor Drive System for Electric Vehicle” under RUSA 2.0. Also, authors thank the the Agencia Nacional de Investigación y Desarrollo (ANID) FONDECYT Regular grant number 1220556, the Research Project PINV01-743 of the Consejo Nacional de Ciencia y Tecnología (CONACYT), ENNOBLE-R02401 and IRCF 24932270 project from the University of Nottingham.

## REFERENCES

[1] T. L. Skvarenina,“The Power Electronics Handbook,” 1st ed., CRC press,2002,pp.664.

[2] Z. Zhou, L. Zhang, Z. Liu, Q. Chen, R. Long, and H. Su, “Model predictive control for the receiving-side DC-DC converter of dynamic wireless power transfer,” *IEEE Trans. Power Electron.*, vol. 35, no. 9, pp. 8985–8997, Sep. 2020, doi: 10.1109/TPEL.2020.69996.

[3] N. Elsayad, H. Moradisizkoohi, and O. A. Mohammed, “A new hybrid structure of a bidirectional DC-DC converter with high conversion ratios for electric vehicles,” *IEEE Trans. Veh. Technol.*, vol. 69, no. 1, pp. 194–206, Jan. 2020, doi: 10.1109/TVT.2019.2950282.

[4] S. A. Gorji, H. G. Sahebi, M. Ektesabi, and A. B. Rad, “Topologies and control schemes of bidirectional DC DC power converters: an overview,” *IEEE Access*, vol. 7, pp. 117997–118019, 2019, doi: 10.1109/ACCESS.2019.2937239.

[5] J. Luo et al., "Novel Cuk-Based Bridgeless Rectifier of Wireless Power Transfer System with Wide Power Modulation Range and Low Current Ripple," *in IEEE Transactions on Industrial Electronics*, vol. 69, no. 3, pp. 2533-2544, March 2022, doi: 10.1109/TIE.2021.3066927.

[6] E. Babaei and M. E. Seyed Mahmoodieh, "Calculation of Output Voltage Ripple and Design Considerations of SEPIC Converter*," in IEEE Trans on Ind Elects*, vol. 61, no. 3, pp. 1213-1222, March. 2014, doi: 10.1109/TIE.2013.2262748.

[7] S- B Wang, Y Zhou, H H C Iu& J- N Chen, “Dynamical behaviour and stability analysis in SEPIC converter based on sliding-mode control”, *Australian Jrl of Electrical & Electronics Engineering*, vol.4,no.1, pp.47-54,2008,doi: 10.1080/1448837X.2008.11464171.

[8] P. K. Maroti, S. Padmanaban, J. B. Holm-Nielsen, M. Sagar Bhaskar, M. Meraj and A. Iqbal, "A New Structure of High Voltage Gain SEPIC Converter for Renewable Energy Applications," *in IEEE Access*, vol. 7, pp. 89857-89868, 2019, doi: 10.1109/ACCESS.2019.2925564.

[9] S. Hasanpour, M. Forouzesh, Y. P. Siwakoti and F. Blaabjerg, "A New High-Gain, High-Efficiency SEPIC-Based DC–DC Converter for Renewable Energy Applications," *in IEEE Jrl of Emerging and Selected Topics in Ind Electron,* vol. 2, no. 4, pp. 567-578, Oct. 2021, doi: 10.1109/JESTIE.2021.3074864.

[10] Dileep G, S. N. Singh & G. K. Singh, “Modelling, design and stability analysis of an improved SEPIC converter for renewable energy systems,” *Int. Jrl of Electron,* vol.104, no.9, pp.1527-1545,2017, doi: 10.1080/00207217.2017.1312709.

[11] Heydari, M., Khoramikia, H. & Fatemi, A, “High-voltage gain SEPIC-based DC–DC converter without coupled inductor for PV systems,” *IET Power Electron*, vol.12, pp.2118-127,2019, doi: 10.1049/iet-pel.2018.5940.

[12] P. Prabhakaran and V. Agarwal, "Novel Boost-SEPIC Type Interleaved DC DC Converter for Mitigation of Voltage Imbalance in a Low-Voltage Bipolar DC Microgrid," *in IEEE Trans. on Ind Electron*, vol. 67, no. 8, pp. 6494-6504, Aug. 2020, doi: 10.1109/TIE.2019.2939991.

[13] P. J. S. Costa, M. V. M. Ewerling, C. H. I. Font and T. B. Lazzarin, "Unidirectional Three-Phase Voltage-Doubler SEPIC PFC Rectifier," *in IEEE Trans. on Power Electron,* vol. 36, no. 6, pp. 6761-6773, June 2021, doi: 10.1109/TPEL.2020.3037480.

[14] P. J. S. Costa; C. H. Illa Font and T. B. Lazzarin, "A family of single phase voltage-doubler high-power-factor SEPIC rectifiers operating in DCM," *IEEE Trans. Power Electron*., vol. 32, no. 6, pp. 4279-4290, Jun. 2017, doi: 10.1109/TPEL.2016.2602940.

[15] B. Singh and A. Anand, "Power Factor Correction in Modified SEPIC Fed Switched Reluctance Motor Drives," *in IEEE Trans. on Industry Appls,* vol. 54, no. 5, pp. 4494-4505, Sept.-Oct. 2018, doi: 10.1109/TIA.2018.2840079.

[16] A. Anand and B. Singh, "Power Factor Correction in Cuk–SEPIC-Based Dual-Output-Converter-Fed SRM Drive," *in IEEE Trans. on Ind Electron.,* vol. 65, no. 2, pp. 1117-1127, Feb. 2018, doi: 10.1109/TIE.2017.2733482.

[17] Priyadarshi, Neeraj & Bhaskar Ranjana, Mahajan & Sanjeevikumar, P. & Blaabjerg, F. & Azam, Farooque, "New CUK–SEPIC converter based photovoltaic power system with hybrid GSA–PSO algorithm employing MPPT for water pumping applications," *IET Power Electron*., vol.13, no. 13, pp. 2824 – 2830, October 2020,doi: 10.1049/iet-pel.2019.1154

[18] Sharma, SK, Pardhi, PK, Saxena, R, "SEPIC for solar energy–based sensorless speed control of induction motor drive," *Int Trans Electr Energ Syst,* vol. 31, no. 12, 2021,doi: 10.1002/2050-7038.13166.

[19] Poovizhi Mani, SenthilKumaran Mahadevan, Anitha Roseline Johnson & Murugesan Kullan , "An optimized design modelling of PV integrated SEPIC-based four-switch inverter for sensorless PMBLDC motor control," *Automatika*, vol.63,no.1,pp. 90-101,2022,doi: 10.1080/00051144.2021.2008621

[20] N. Guler, S. Biricik, S. Bayhan and H. Komurcugil, "Model Predictive Control of DC–DC SEPIC Converters With Autotuning Weighting Factor," *in IEEE Transactions on Ind., Electron.,* vol. 68, no. 10, pp. 9433-9443, Oct. 2021, doi: 10.1109/TIE.2020.3026301.

[21] J. J. Vásquez S., J. A. Domínguez A., M. Espinosa T., M. A. Alonso P., E. Y. Mendoza and J. L. Flores, "Passivity Based-Control of Output Voltage Regulation with MPPT for Photovoltaic Panel Using two SEPIC Converters," 2020 *IEEE International Autumn Meeting on Power Electron., and Computing (ROPEC*), Ixtapa, Mexico, pp. 1-6, 2020, doi: 10.1109/ROPEC50909.2020.9258757.

[22] El Khateb, A., Rahim, N. A., Selvaraj, J., & Uddin, M. N., "Fuzzy-logic-controller-based SEPIC converter for maximum power point tracking." *IEEE Trans., on Industry Applications*.," vol. 50, no.4, pp.2349-2358, 2014, doi: 10.1109/TIA.2014.2298558.

[23] Utkin, Vadim & Guldner, Juergen & Shi, Jingxin, *Sliding Mode Control in Electro-Mechanical Systems*, 2nd ed., CRC press, 2009, pp.503.

[24] Shtessel, Y.B., Edwards, C., Fridman, L.M., & Levant, A, *Sliding Mode Control and Observation*, 1st ed. Birkhäuser New York, NY,2013, pp.356.

[25] F. Torelli, P. Montegiglio, G. Piccinni and G. Acciani, "SMC-inspired Control Approach Applied to DC-Motor Drives," *2020 IEEE Int.Conf. on Environment and Electrical Engineering and 2020 IEEE Industrial and Commercial Power Systems Europe (EEEIC / I&CPS Europe)*, Madrid, Spain, 2020, pp. 1-6. doi: 10.1109/EEEIC/ICPSEurope49358.2020.9160764.

[26] V. Utkin, "Discussion Aspects of High-Order Sliding Mode Control," *IEEE Trans. on Aut., Ctrl*, vol. 61, no. 3, pp. 829-833, March (2016), doi: 10.1109/TAC.2015.2450571.

[27] Leonid Fridman., Jean-Pierre Barbot.,Franck Plestan., "Recent Trends in Sliding Mode Control," *IET Ctrl, Robotics and Sensors Series*, pp.504,2016.

[28] Dhanasekar Ravikumar & Ganesh Kumar Srinivasan, "Implementation of higher order sliding mode control of DC–DC buck converter fed permanent magnet DC motor with improved performance," *Automatika*, vol.64,no.1, pp.162-177,2023, doi:10.1080/00051144.2022.2119499.

[29] Zhang X, Li J, Ma Z, Chen D, Zhou X, "Lateral Trajectory Tracking of Self-Driving Vehicles Based on Sliding Mode and Fractional-Order Proportional-Integral-Derivative Control," *Actuators*, vol.13, no.1,pp.7 2024, doi:10.3390/act13010007.

[30] Camacho C, Alvarez H, Espin J, Camacho O, "An Internal Model Based—Sliding Mode Control for Open-Loop Unstable Chemical Processes with Time Delay," *ChemEngg,* vol.7. no.3, pp.53, 2023, doi: 10.3390/chemengineering7030053.

[31] García Torres CJ, Ferré Covantes LA, Vaca García CC, Estrada Gutiérrez JC, Guzmán AN, Acosta Lúa C. "A Lyapunov Stability Analysis of Modified HOSM Controllers Using a PID-Sliding Surface Applied to an ABS Laboratory Setup," *Applied Sciences*, vol.12, no.8, pp.3796, 2022, doi:10.3390/app12083796.

[32] Arie Levant, "Homogeneity approach to high-order sliding mode design," *Automatica*, vol.41, no.5, pp. 823-830, 2005, doi: 10.1016/j.automatica.2004.11.029.

[33] H. Komurcugil, S. Biricik, S. Bayhan and Z. Zhang, "Sliding Mode Control: Overview of Its Applications in Power Converters," *in IEEE Ind., Elects Mgz*, vol. 15, no. 1, pp. 40-49, March 2021, doi: 10.1109/MIE.2020.2986165.

**R. Dhanasekar** graduated with Electrical and Electronics engg degree from RVS college of Engg and tech,Tamilnadu, India, 2004, Masters in Power electronics and drives from Mepco Schlenk Engineering college, Tamilnadu, India, 2006 and completed the PhD degree at CEG,Anna University, Chennai, Tamilnadu, India. Currently, he is an Associate Professor at Sri Sairam Institute of Technology, Chennai, Tamilnadu.

**S. Ganesh Kumar** professor in DEEE, CEG, Anna University, Chennai, India has published 31 journals, 32 conference papers,8 book chapters, 1 book and 3 patents. He completed two research projects with Rs 27 Lakhs and presently doing two projects of worth Rs 3 Crores.

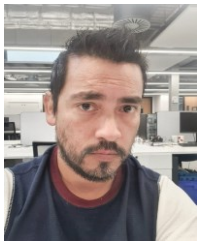

**Marco Rivera** (Senior Member, IEEE) holds degrees in civil engineering and electrical engineering from the Universidad de Concepción, as well as a Ph.D. in electronic engineering from the Universidad Técnica Federico Santa Maria. He has directed and participated in a number of projects funded by the National Fund for Scientific and Technological Development (FONDECYT), the National Commission for Scientific and Technological Research (Comisión Nacional para la Investigación Cientfica y Técnica, CONICYT), and the Paraguayan Program for the Development of Science and Technology (PRDCT). He is also a Full Professor at the Universidad de Talca's Department of Electrical Engineering.